RSC Advances

This is an *Accepted Manuscript*, which has been through the Royal Society of Chemistry peer review process and has been accepted for publication.

Accepted Manuscripts are published online shortly after acceptance, before technical editing, formatting and proof reading. Using this free service, authors can make their results available to the community, in citable form, before we publish the edited article. This *Accepted Manuscript* will be replaced by the edited, formatted and paginated article as soon as this is available.

You can find more information about *Accepted Manuscripts* in the **Information for Authors**.

ROYAL SOCIETY OF CHEMISTRY

www.rsc.org/advances

Enhanced encapsulation of superparamagnetic Fe₃O₄ in acidic core-containing micelles for magnetic resonance imaging

Depannita Biswas,[#] Puzhen Li,[#] Dapeng Liu,[§] Jung Kwon Oh[#]*

Department of Chemistry and Biochemistry, Centre for NanoScience Research, Concordia University, Montreal, Quebec, Canada H4B 1R6

§ Department of Chemistry and Waterloo Institute for Nanotechnology, University of Waterloo, Waterloo, ON, Canada N2L 3G1.

Tel: 1-514-848-2424 ext 5306, email: john.oh@concordia.ca

ABSTRACT

We report the synthesis of well-controlled amphiphilic block copolymer having pendant carboxylic acid groups in the hydrophobic block (BCP-HY) by a combination of controlled radical polymerization and partial hydrolysis. Aqueous micellization of the block copolymer in the presence of hydrophobic superparamagnetic iron oxide nanoparticles (SNPs) results in the formation of magnetic nanoassembled structures with acidic cores. Compared with the counterparts having neutral cores, the resulting SNP/BCP-HY micelles retain greater loading level of SNPs due to the ability of the acidic cores to anchor to SNP surfaces, thus providing dark magnetic resonance imaging (MRI) contrast enhancement. Further, they exhibit good colloidal stability in physiological conditions and in the presence of proteins, as well as promisingly show acidic pH-responsive enhanced release of encapsulated doxorubicin (an anticancer drug). These results suggest that the SNP/BCP-HY micelles having acidic cores have great potential for theranostics with treatment (anticancer drug delivery) and diagnosis based on MRI.

INTRODUCTION

Magnetic resonance imaging (MRI) is considered as a powerful and non-invasive molecular imaging modality that provides high resolution and excellent soft-tissue contrast based on the stimulation and interaction of hydrogen protons.[1] To enhance the sensitivity and quality of MRI, the use of exogenous contrast agents that enable the induced change in relaxation time of protons in immediate surrounding is required.[2, 3] It is known that the effect of contrast agents on MRI is assessed based on their ability to alter longitudinal (spin-lattice) T_1 relaxation time and transverse (spin-spin) T_2

relaxation time. Particularly, T_2-weighted MRI contrast agents shorten T_2 transverse relaxation time of water protons, providing negative (dark) contrast images. Superparamagnetic iron oxide nanoparticles (SNPs) such as magnetite (Fe_3O_4) and maghemite (γ-Fe_2O_3) are commonly employed as biocompatible MRI contrast agents.[4-8] Numerous studies suggest that the size of SNPs is the important parameter for developing SNPs as bright imaging (T_1-weighted) and dark imaging (T_2-weighted) contrast agents.[9-13] This is because their relaxivities ($r_1 = 1/T_1$ and $r_2 = 1/T_2$) are varied with their particle sizes and magnetic moments.[14-16] A common approach to dark MRI contrast enhancement is the design of SNPs with larger sizes.[17-20] An alternative is the development of magnetic clusters of SNPs in nanocompartments as crosslinked nanogels,[21, 22] amphiphilic lipids,[23, 24] and nanoaggregates.[25-28]

Of particular interests is the magnetic micellar aggregates self-assembled from amphiphilic block copolymers in the presence of hydrophobic SNPs. Well-designed magnetic aggregates not only provide T_2-weighted MRI contrast enhancement, but also have all benefits as drug delivery nanocarriers. These "theranostic nanomedicines" endow simultaneous treatment and real-time imaging of target sites, particularly tumor tissues.[29, 30] A number of SNP-loaded micelles based on amphiphilic block copolymers have been reported. The amphiphilic block copolymers have been designed to have hydrophobic groups or polymeric chains that are either covalently attached to hydrophilic poly(ethylene glycol) (PEG)[31-34] or grafted from polysaccharides.[35-37] Furthermore, novel multifunctional block copolymers with stimuli-responsive properties exhibiting enhanced drug release have been reported.[38-40] However, most of conventionally-designed magnetic micelles utilize hydrophobic-hydrophobic interaction of SNPs with hydrophobic blocks to encapsulate SNPs in hydrophobic cores; accordingly, this process presents potential challenges to poor colloidal stability in shelf and premature release of encapsulated SNPs during blood circulation.

Herein, we demonstrate that an introduction of pendant carboxylic acid groups in the hydrophobic cores can circumvent the challenges, and further promote the enhanced encapsulation of SNPs in acidic cores due to stronger binding affinity of acidic groups to SNP surfaces. A model amphiphilic block copolymer consisting of a hydrophilic PEG block and a hydrophobic methacrylate block containing pendant carboxylic acids was synthesized by a combination of atom transfer radical polymerization and hydrolysis, thus PEG-b-P(tBMA-co-MAA) (BCP-HY) (tBMA: t-butyl methacrylate and MAA: methacrylic acid). This amphiphilic block copolymer self-assembled to form micellar aggregates at concentrations above critical micellar concentration. In the presence of hydrophobic SNPs, the process yielded magnetic micelles with enhanced encapsulation of SNPs. The resulting magnetic micelles exhibit T_2-weighted dark MRI contrast enhancement, great colloidal

stability in physiological conditions and in the presence of proteins, as well as enhanced release of encapsulated doxorubicin (an anticancer drug) in acidic pH.

EXPERIMENTAL

Instrumentation and analyses. ^{1}H-NMR spectra were recorded using a 500 MHz Varian spectrometer. The CDCl$_3$ singlet at 7.26 ppm and DMSO-d$_6$ quintet at 2.50 ppm was selected as the reference standard. Monomer conversion was determined using ^{1}H-NMR. Molecular weight and molecular weight distribution were determined by gel permeation chromatography (GPC). An Agilent GPC was equipped with a 1260 Infinity Isocratic Pump and a Refractive Index (RI) detector. Two Agilent columns (PLgel mixed-D and mixed-C) were used with DMF containing 0.1 mol% LiBr at 50 °C at a flow rate of 1.0 mL/min. Linear poly(methyl methacrylate) standards from Fluka were used for calibration. Aliquots of polymer samples were dissolved in DMF/LiBr. The clear solutions were filtered using a 0.45 μm PTFE filter to remove any DMF-insoluble species. A drop of anisole was added as a flow rate marker. The hydrodynamic diameter by volume of SNPs and self-assembled micellar aggregates were measured by dynamic light scattering (DLS) at a fixed scattering angle of 175° at 25 °C with a Malvern Instruments Nano S ZEN1600 equipped with a 633 nm He-Ne gas laser. Zeta potential (ξ) of aqueous SNP/BCP-HY micellar dispersions were measured using Malvern Zetasizer Nano ZSP equipped with a 633 nm He-Ne laser. Fluorescence spectra on a Varian Cary Eclipse Fluorescence spectrometer and UV/Vis spectra on an Agilent Cary 60 UV/Vis spectrometer were recorded using a 1 cm wide quartz cuvette.

Transmission Electron Microscopy (TEM). TEM images were taken using a Philips CM10 TEM, operated at 60 kV. An AMT V601 DVC camera with point to point resolution and line resolution of 0.34 nm and 0.20 nm respectively was used to capture images at 3200 by 4668 pixels. To prepare specimens, the micellar dispersions were dropped onto copper TEM grids (200 mesh, carbon-coated), blotted and then allowed for air-drying at room temperature.

Thermogravimetric analysis (TGA). Thermogravimetric analysis (TGA) measurements were carried out using a TA Instruments Q50 analyzer. Typically, the dialyzed and lyophilized SNP/BCP-HY micelles (5−10 mg) were placed onto a platinum pan, and the sample was heated from 25 to 800 °C at a heating rate of 20 °C per minute under nitrogen flow.

Materials. Copper(II) bromide (CuBr$_2$, >99.99%), tin(II) 2-ethylhexanoate (Sn(EH)$_2$, 95%), iron(II) chloride (FeCl$_2$, 98%), iron(III) chloride (FeCl$_3$, 97%), oleic acid (97%), nile red (NR), triethylamine

(Et$_3$N, > 99.5%), trifluoroacetic acid (CF$_3$COOH, 99%), and doxorubicin hydrochloride (DOX, -NH$_3^+$Cl$^-$ salt form, >98%) from Sigma-Aldrich as well as potassium hydrogen phthalate (KHP) and bovine serum albumin (BSA> 95%) from MP Biomedicals were purchased and used as received. Dialysis tubing with MWCO = 12 kDa from Spectrum Labs and Pierce® BCA Protein Assay Kit from Thermo Scientific were purchased. Tertiary-butyl methacrylate (tBMA) from Aldrich was purified by passing through a column filled with basic alumina to remove inhibitors before use. PEG-functionalized 2-bromoisobutyrate with EO # =113 (PEG-Br),[41] tris(2-pyridylmethyl)amine (TPMA),[42] and oleic acid-stabilized SNPs (OA-SNPs)[43] were synthesized according to literature procedure.

Synthesis of PEG-b-PtBMA by ARGET ATRP. PEG-Br (56.2 mg, 113 µmol), tBMA (4 g, 28 mmol), CuBr$_2$ (2.9 mg, 5.6 µmol), and TPMA (3.3 mg, 11.3 µmol) were mixed with anisole (17.5 g) in a 50 mL Schlenk flask. The resulting organic mixture was deoxygenated by purging under nitrogen for 30 min and then immersed in a preheated oil bath at 40 °C. A nitrogen pre-purged solution of Sn(EH)$_2$ (7.3 mg, 45 µmol) dissolved in anisole (2 g) was injected into the Schlenk flask to initiate polymerization. After 4.5 hrs, the polymerization was stopped by cooling the reaction mixture in an ice bath and exposing it to air.

For purification, the as-synthesized polymer solution was precipitated from cold hexane three times to remove un-reacted monomers. The precipitates were dissolved in acetone and then passed through a column filled with basic alumina to remove residual copper species. The polymer solution was passed through a 0.45 µm PTFE filter to remove residual tin species. Solvents were removed by rotary evaporation and the residues were further dried in a vacuum oven at room temperature for 24 hrs, yielding the purified, dried PEG-b-PtBMA (BCP-HY-0) block copolymer.

Partial hydrolysis to synthesize PEG-b-P(tBMA-co-MAA) (BCP-HY). For hydrolytic cleavage of t-butoxy groups in the PtBMA blocks under acidic conditions, the purified, dried PEG-b-PtBMA (0.1 g, 5.9 µmol tBMA units) dissolved in dichloromethane (DCM, 1.5 mL) was mixed with different amounts of CF$_3$COOH and stirred for 18 hrs at room temperature. The reaction mixtures were precipitated from cold hexane three times, and then the precipitates were dried in vacuum oven for 12 hrs at room temperature.

Determination of critical micellar concentration (CMC) using a NR probe. A stock solution of NR in THF at 1 mg/mL and a stock solution of BCP-HY-45 in THF at 1 mg/mL and 5 µg/mL were prepared. Different amounts of the BCP-HY-45 stock solution were mixed with the same amount of the NR stock solution (0.5 mL). After the final volume of the resulting mixtures was adjusted to be 2

mL with additional THF, water (10 mL) was added. The resulting dispersions were stirred for 24 hrs to remove THF. Gas chromatography was used to confirm there was no residual THF remaining in the micellar dispersions. Excess NR was removed by filtration using 0.45μm PES filters to yield a series of NR-loaded micelles at various concentrations of BCP-HY-45 ranging from 10^{-6} to 0.1 mg/mL. Their fluorescence spectra were recorded with λ_{ex} = 480 nm to monitor the fluorescence intensity at maximum λ_{em} = 620 nm. Similar procedure was used for BCP-HY-0.

Preparation and characterization of aqueous SNP/BCP-HY micelles. An organic solution of BCP-HY (20 mg) dissolved in THF (3 mL) was mixed with various amount of OA-SNP. The resulting solutions were added drop-wise to water (30 mL) under magnetic stirring. The resulting dispersions were stirred for 30 min at room temperature, and then dialyzed against water (1 L) for 2 days, yielding aqueous SNP/BCP-HY micellar dispersions at 0.7 mg/mL concentration. After the removal of black precipitates undesirably formed during dialysis, the dispersions were subjected to centrifugation (6000 rpm, 25 min, 4 °C), followed by lyophilization using a freeze-drier. The dried products were analyzed by TGA. The loading level of SNPs in micelles was determined by the weight ratio of SNPs in dried solids to dried polymers.

Relaxivity Measurements. Aqueous SNP/BCP-HY micelles at 1 mg/mL was diluted with different volumes of distilled water at volume ratio of dispersion/water = 1/0, 2/1 and 1/2 v/v. The dispersions were then dispensed into 7.5 mm o.d. NMR tubes. Their longitudinal and transversal relaxation times (T_1 and T_2) were measured with a dedicated NMR relaxometer (Bruker Minispec 60 mq, 60 MHz, 1.41 T) at 37 °C. The Fe content in the dispersions was also precisely determined by Inductively-Coupled Plasma (ICP, Agilent 7500ce). Prior to ICP measurements, samples of each dispersion were digested overnight at 80 °C in HNO_3 (trace metal, Fisher Scientific A509−500) and 30% H_2O_2 (Sigma-Aldrich).

Cell viability using MTT assay. Human embryonic kidney (HEK 293T) and HeLa cancer cells were cultured in DMEM (Dulbecco's modified Eagle's medium) containing 10% FBS (fetal bovine serum) and 1% antibiotics (50 units/mL penicillin and 50 units/mL streptomycin) at 37 °C in a humidified atmosphere containing 5% CO_2. Cells were plated at 5 x 10^5 cells/well into a 96-well plate and incubated for 24 hrs in DMEM (100 μL) containing 10% FBS for the following experiments. They were then incubated with various concentrations of SNP/BCP-HY micellar dispersions for 48 hrs. Blank controls without micelles (cells only) were run simultaneously. Cell viability was measured using CellTiter 96 Non-Radioactive Cell Proliferation Assay kit (MTT, Promega) according to manufacturer's instruction. Briefly, 3-(4,5-dimethylthiazol-2-yl)-2,5-diphenyltetrazolium bromide

(MTT) solutions (15 µL) was added into each well. After 4 hrs of incubation, the medium containing unreacted MTT was carefully removed. DMSO (100 µL) was added into each well in order to dissolve the formed formazan blue crystals, and then the absorbance at $\lambda = 570$ nm was recorded using Powerwave HT Microplate Reader (Bio-Tek). Each concentration was 12-replicated. Cell viability was calculated as the percent ratio of absorbance of mixtures with micelles to control (cells only).

Colloidal stability of SNP/BCP-HY-45 micelles in the presence of proteins. Aliquots of SNP/BCP-HY-45 micellar dispersion (1 mg/mL) were mixed with an aqueous BSA solution in PBS at pH = 7.4 (40 mg/mL) at mass ratio = 40/1 and 1/1 wt/wt of BSA to SNP/BCP-HY-45 micelles. The resulting mixtures were incubated at 37 °C and analyzed using DLS at 24 hrs and 48 hrs. They were then subjected to centrifugation (12,000 rpm x 25 min) to precipitate any BSA-micelle aggregates undesirably formed during incubation due to colloidal instability. The concentration of BSA in supernatant was determined using BCA assay according to instruction manual. Briefly, aliquots of the supernatants (25 µL) were transferred into a 96-well plate and mixed with BCA reagent (200 µL). Blank controls (BSA only) were run simultaneously. The mixtures were incubated at 37 °C for 30 min. Their absorbance was measured at $\lambda = 562$ nm using a Powerwave HT Microplate Reader (Bio-Tek). The percentage of free BSA was calculated as the weight ratio of BSA in the supernatants of the mixtures to that in control (BSA only).

Colloidal stability of SNP/BCP-HY-45 micelles at various pH conditions. Aliquots of aqueous SNP/BCP-HY-45 micelles (1 mL) were mixed with an equal volume (1 mL) of KHP buffer (pH = 3 and 5.2), PBS (pH = 7.4 and 9.0). DLS was used to follow any changes in their size distributions.

Preparation of Dox-loaded micelles. Water (10 mL) was added drop-wise to an organic solution consisting of the BCP-HY-45 (20 mg), Dox (2 mg, 3.4 µmol), and Et$_3$N (1.4 mg, 13.7 µmol) in DMF (2 mL). The resulting dispersion was stirred for 1 hr, and then dialyzed against water (1 L) for 1 day, yielding Dox -loaded micellar dispersion at 1.7 mg/mL concentration. To determine the loading level of Dox using UV/Vis spectroscopy, an aliquot of aqueous Dox -loaded micellar dispersion (1 mL) were mixed with DMF (5 mL) to form a clear solution consisting of the DMF/water mixture (5/1 v/v). Their UV/Vis spectra were recorded and the loading level of Dox was calculated by the weight ratio of loaded Dox to dried polymers.

Acidic pH-responsive Dox release. Aliquots of Dox-loaded micellar dispersion (2 mL) were transferred into dialysis tubing, immersed in PBS (40 mL) at pH = 7.4 and KHP buffer solution (40 mL) at pH = 5.2. Fluorescence spectrum of outer solution was measured over 30 hrs at $\lambda_{ex} = 470$ nm.

To quantify %Dox release from Dox-loaded micelles, the amount of Dox equivalent to Dox encapsulated in Dox-loaded micellar dispersion (2 mL) was dissolved in buffer solutions at pH = 7.4 and 5 (40 mL) and their fluorescence spectra were measured.

RESULTS AND DISCUSSION

Synthesis and partial hydrolysis of PEG-b-PtBMA. As illustrated in **Figure 1a**, our approach to synthesize well-defined PEG-b-PtBMA utilizes atom transfer radical polymerization of tBMA medicated with $CuBr_2$/TPMA complex in the presence of PEG-Br initiator in anisole at 40 °C. After being purified by precipitation from hexane, the dried, purified PEG-b-PtBMA was characterized with a molecular weight as a number average molecular weight (M_n) = 18.7 kg/mol with M_w/M_n = 1.1 by GPC (**Figure S1**). The M_n being larger than that of PEG-Br initiator (10.9 kg/mol) along with no significant traces of residual PEG-Br in the GPC trace suggest the successful chain extension of PtBMA from PEG-Br. ^{1}H-NMR spectrum in **Figure 1b** shows the typical peaks at 3.5-3.7 ppm corresponding to EO protons in the PEG block and a peak at 1.5 ppm (b) corresponding to t-butoxy protons in the PtBMA block. The integral ratio of these peaks [(b/9)/(EO/4)], combined with #EO of PEG = 113, allows for the determination of the degree of polymerization (DP) of the PtBMA block to be 84, thus, forming PEG_{113}-b-$PtBMA_{84}$.

Reports describe the hydrolytic cleavage (hydrolysis) of pendant t-butoxy groups of PtBMA to the corresponding poly(methacrylic acid) (PMAA).[44] Here, the hydrolytic cleavage of PEG-b-PtBMA was examined in the presence of various amounts of CF_3COOH as the mole ratios of $[CF_3COOH]_0$/[tBMA in PtBMA block]$_0$. As seen in a typical ^{1}H-NMR spectrum in **Figure 1b**, the decrease of the peak (b) resulting from the hydrolytic cleavage of t-butoxy groups was utilized to calculate the hydrolysis (%). As summarized in **Table 1**, a series of well-controlled PEG-b-P(tBMA-co-MAA) (BCP-HY) with different densities of pendant carboxylic acids (-COOH) was synthesized by a combination of ATRP and partial hydrolysis. Interestingly, the cleavage of pendant t-butoxy groups linearly increased with an increasing amount of CF_3COOH (**Figure S2**).
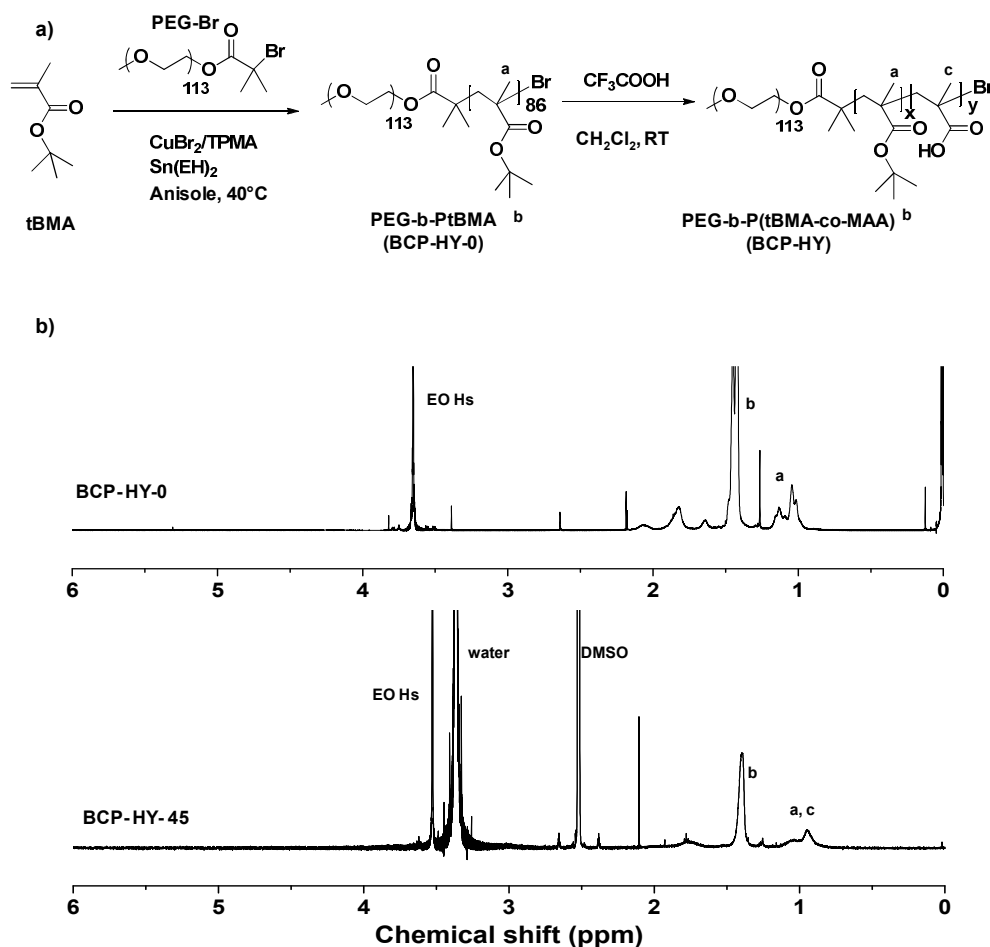
Figure 1. Our approach to synthesize well-controlled PEG-b-P(tBMA-co-MAA) having pendant carboxylic acids by a combination of atom transfer radical polymerization and partial hydrolytic cleavage (a) and ^{1}H-NMR spectra of PEG-b-PtBMA (BCP-HY-0) in CDCl$_3$ and PEG-b-P(tBMA-co-MAA) (BCP-HY-45) in DMSO-d$_6$ (b). Conditions for ATRP: [tBMA]$_o$/[PEG-Br]$_o$/[CuBr$_2$]$_o$/[TPMA]$_o$/[Sn(EH)$_2$]$_o$ = 250/1/0.05/0.15/0.4; tBMA/anisole = 1/4 wt/wt at 40 °C.

Table 1. Characteristics and properties of PEG-b-P(tBMA-co-MAA) (BCP-HY) copolymers prepared by partial hydrolytic cleavage of pendant PtBMA block in dichloromethane.

BCP-HY	[CF$_3$COOH]$_0$ /[tBMA]$_0$	DP[a]		Hydrolysis[b] (%)
		PtBMA	PMAA	
BCP-HY-0	0/1	84	0	0
BCP-HY-25	2/1	63	21	25
BCP-HY-45	3/1	46	38	45
BCP-HY-85	5/1	11	73	85
BCP-HY-97	10/1	2	82	97

a) Determined by ^{1}H-NMR, b) Calculated by DP of PtBMA and PMAA using the equation of DP(PMAA)/[DP(PtBMA)+DP(PMAA)]

Aqueous micellization of BCP-HY copolymers. The resulting PEG-b-PtBMA block copolymer (BCP-HY-0) consisting of hydrophilic PEG (29 wt%) and hydrophobic PtBMA (71 wt%) is amphiphilic. The critical micellar concentration (CMC) in aqueous solution was determined using Nile Red (NR) as a fluorescence probe.[45] A series of aqueous mixture consisting of the same amount of NR and various amounts of BCP-HY-0 were prepared. From their fluorescence spectra, a plot of fluorescence intensity at maximum wavelength (λ_{max}) against BCP-HY-0 concentration was constructed (**Figure 2**). Regression analysis of the two linear regions of the data allows for the determination of CMC to be 7 µg/mL.

The partial hydrolytic cleavage of PtBMA to the corresponding PMAA gradually changes the hydrophobicity of PtBMA cores to be relatively hydrophilic. Eventually, the formed BCP-HY copolymers with higher MAA units in P(tBMA-co-MAA) blocks behave to be double hydrophilic, and thus have less or no ability to form micellar aggregates in aqueous solution. However, the BCP-HY with less hydrolysis could self-assemble to form micellar aggregates. Typically, the CMC of BCP-HY-45 (45% PtBMA hydrolyzed) was determined to be 20 µg/mL. These results suggest that the CMC ranges between 7-20 µg/mL for BCP-HY copolymers formed at 0-45% hydrolysis.

Further, the fluorescence maximum wavelength of NR encapsulated in BCP-HY-45 micelles was λ_{max} = 620 nm, which is larger by 20 nm than that (λ_{max} = 600 nm) of NR encapsulated in BCP-HY-0 micelles (**Figure S3**). As reported,[46] such red-shift is attributed to increasing hydrophilicity of P(tBMA-co-MAA) cores in BCP-HY-45 micelles, compared to PtBMA cores in BCP-HY-0 micelles.
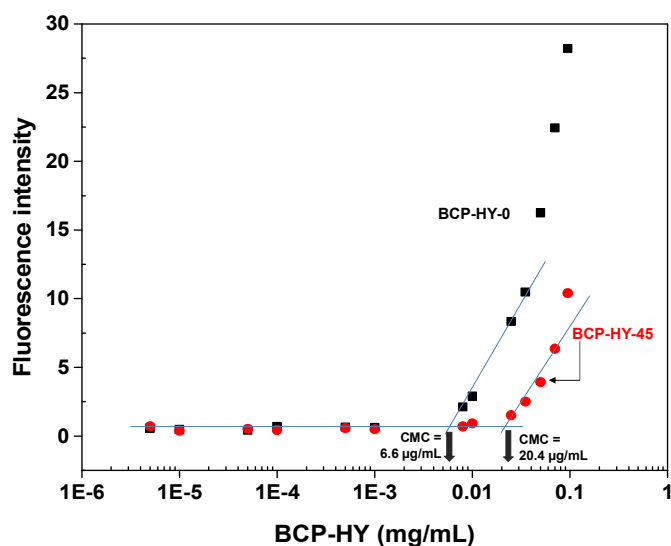
Figure 2. Fluorescence intensity of NR at λ_{max} in aqueous mixture of BCP-HY-0 and BCP-HY-45 to determine CMC.

Encapsulation of SNPs through aqueous micellization. OA-stabilized SNPs (OA-SNPs) were synthesized by co-precipitation of Fe(II) and Fe(III) in the presence of OA in a water/ethanol/toluene, purified by precipitation from EtOH, and then dispersed in hexane at 1 mg/mL. The average diameter was determined to be 3.5 nm by TEM and 9 nm by DLS in hexane. The detailed synthesis and characterization is described in our previous publication.[43] OA-SNPs were physically encapsulated in BCP-HY micelles through self-assembly of BCP-HY in the presence of OA-SNPs in aqueous solution. An organic solution consisting of OA-SNPs and BCP-HY dissolved in THF was added dropwise into water under magnetic stirring. The mixtures were subjected to intensive dialysis to remove THF, allowing for the formation of self-assembled micellar aggregates encapsulated with SNPs in the hydrophobic micellar cores. After the removal of black precipitates unexpectedly formed during aqueous micellization inside the dialysis tubing, the resulting aqueous dispersions were subjected to centrifugation to further eliminate large aggregates (see **Figure S4** for DLS histograms before and after centrifugation as an example). In this way, aqueous dispersions of well-defined SNP/BCP-HY micelles with monomodal distribution were prepared. SNP/BCP-HY micelles were then characterized for average diameters by DLS. The dispersions were further lyophilized to quantitatively determine the content of SNPs in micellar cores using TGA.

The amount of OA-SNPs in the feed was varied in order to determine the appropriate weight ratio of SNP/BCP-HY for aqueous micellization. With BCP-HY-0 as a control, its given amount was mixed with various amounts of OA-SNPs. When the wt ratio of SNP/BCP-HY-0 increased from 0/1 to 2/1(i.e. an increasing amount of SNPs), the diameter of the resulting SNP/BCP-HY-0 micelles increased from 38 to 81 nm, and then was likely to reach plateau (**Figure 3a and S5a**). Further, obtained from TGA measurements (**Figure S5b**), the SNP content in micellar cores increased with an increasing ratio of SNP/BCP-HY-0 in the feed (**Figure 3b**). However, the loading efficiency was sacrificed from 67 to 43%. These results suggest the formation of larger micellar aggregates with higher loading level of SNPs, as the amount of SNP increased in the feed. Considering the loading level and efficiency of SNPs in micellar cores, the weight ratio of OA-SNPs/BCP = 1.5/1 was selected for further study.
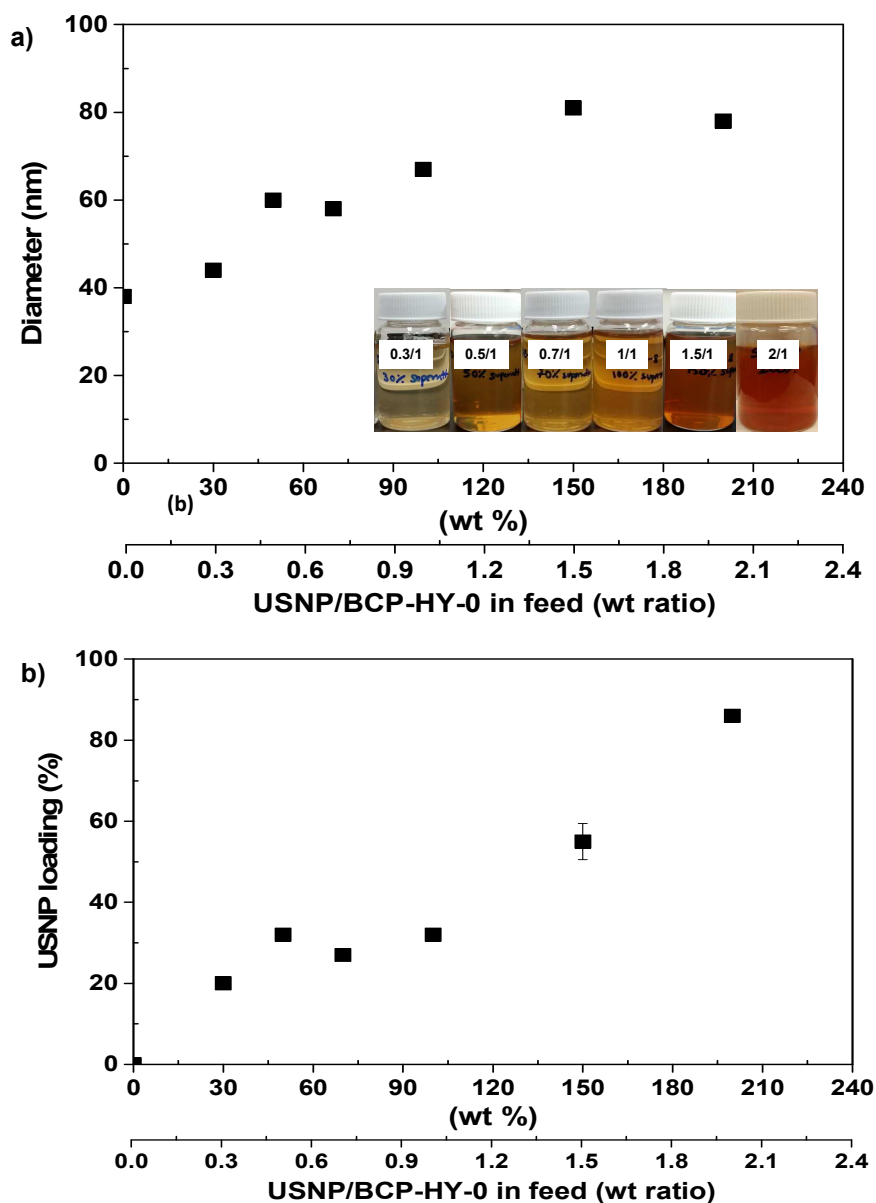
Figure 3. Evolution of diameter by DLS (a) and SNP loading level by TGA (b) of SNP/BCP-HY-0 micelles prepared with various wt ratios of SNPs/BCP-HY-0 in the feed. Inset of a): digital images of micellar dispersions.

Adopting the ratio, aqueous micellization of partially-hydrolyzed BCP-HY-45 amphiphilic block copolymer in the presence of OA-SNPs was examined to synthesize SNP/BCP-HY-45 micellar aggregates. Their size and morphology were analyzed by DLS and TEM (**Figure 4**). They had the diameter = 55 nm by DLS. Using the TGA data, the loading level of SNPs was estimated to be 77%. As compared in **Figure 5**, the SNP loading level encapsulated in BCP-HY-45 micelles (containing pendant acids) is higher by 20%, than that in BCP-HY-0 micelles (with no pendant acids). The higher

loading level is plausibly due to the presence of pendant carboxylic acids in BCP-HY-45 micelles that can anchor to SNP surfaces with greater binding affinity, and the hydrophobic PtBMA segments contributing to the physical entrapment of SNP in hydrophobic cores. Such combination could have a synergistic effect and provide enhanced SNP loading in micellar cores during aqueous micellization. With a promising result, the SNP/BCP-HY-45 micelles were evaluated for magnetic properties and colloidal stability.
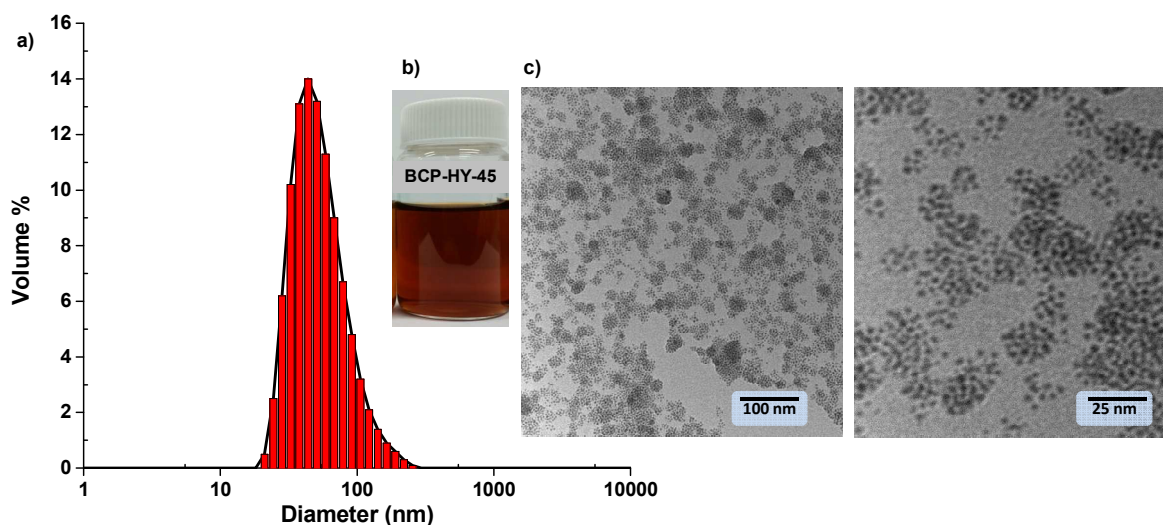
Figure 4. DLS diagram (a), digital image (b), and TEM images (c) with different magnifications of SNP/BCP-HY-45.
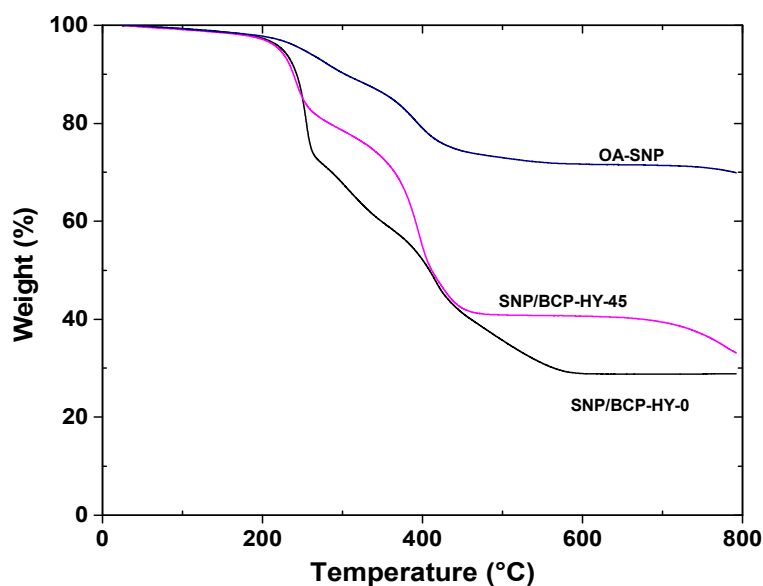
Figure 5. TGA diagram of the purified, lyophilized SNP/BCP-HY-45 micelles, compared with those of SNP/BCP-HY-0 micelles and OA-SNPs.

Relaxometric properties of SNP/BCP-HY micelles. SNPs are known for the use as negative contrast agents in MRI (dark imaging) due to their ability to shorten transverse relaxation time (T_2) of water protons.[47] The relaxometric properties of SNP/BCP-HY-45 micelles in aqueous media were measured at clinical magnetic field strength of 1.41 T (corresponding to 60 MHz) at 37 °C. Their T_1 and T_2 relaxation times were measured at different Fe concentrations. From the slopes of the plots of $1/T_1$ and $1/T_2$ relaxation rates vs Fe contents (**Figure 6a**), transversal relaxivity constant $r_2 = 71.0$ mM^{-1}s^{-1} and thus relaxometric ratio of $r_2/r_1 = 54.2$ were calculated, suggesting their capability for T_2-weighted contrast enhancement. To get more insight into the relaxometric properties of SNP/BCP-HY micelles, other SNP/BCP-HY-0 micelles prepared with different diameters were further tested (**Figure S6**) and their relaxivity constants were determined using the similar protocol (**Table 2**). One observation is the good correlation of r_2 relaxivity constant with micelle diameter. As shown in **Figure 6b**, the r_2 value decreased from 91 to 71 mM^{-1}s^{-1} as the diameter of SNP/BCP-HY micelles decreased from 91 to 55 nm. Such decrease of r_2 value is presumably due to less clustering effect of SNPs in smaller-sized micelles that contain less SNPs in each micelle. Another observation is that the r_2 value of SNP/BCP-HY-45 micelles is smaller than that of SNP/BCP-HY-0 micelles even though the loading level of SNPs is greater in SNP/BCP-HY-45 micelles than the other. This is plausibly due to the surface properties of micelles that are accessible to water molecules,[48] in addition to the size effect. The r_2 relaxivity constant for SNP/BCP-HY micelles ranged at 70-90 mM^{-1}s^{-1}. The core diameter of SNPs used in this work is 3.5 nm by TEM. As reported, the r_2 value can be increased with the use of SNPs with larger diameters.[31]
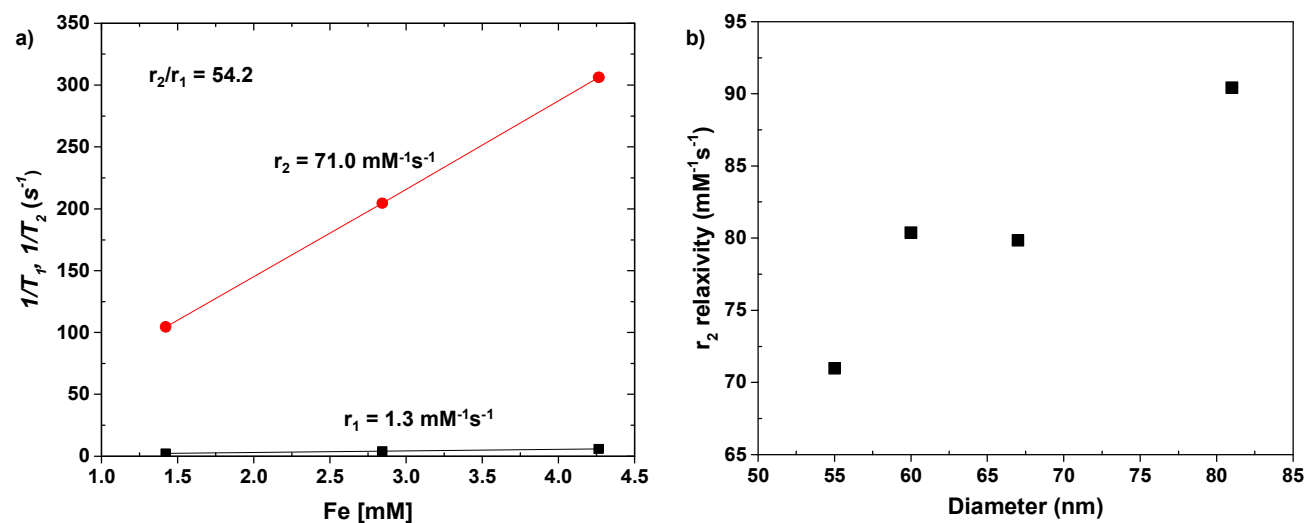
Figure 6. Relaxation rates ($1/T_1$ and $1/T_2$) versus Fe concentration for SNP/BCP-HY-45 micelles (a) and dependence of r_2 relaxivity constant with diameter of SNP/BCP-HY micelles (b) at 1.41 T and 37 °C.

Table 2. Physical and magnetic properties of various SNP/BCP-HY micelles.

Sample name	SNPs (%)		D_h (nm)	r_2 (mM^{-1}s^{-1})	r$_2$/r$_1$
	In feed	In micelles			
SNP/BCP-HY-0/0.5	50	32	60	80.4	143.5
SNP/BCP-HY-0/1	100	32	67	79.9	128.8
SNP/BCP-HY-0/1.5	150	55	81	90.4	161.5
SNP/BCP-HY-45/1.5	150	76	55	71.0	54.2

Cytotoxicity. To preliminarily assess aqueous SNP/BCP-HY micelles toward MRI applications, *in vitro* cytotoxicit*y* with both HEK 293T and HeLa cancer cells were examined using MTT assay (a calorimetric method to measure cell toxicity). Aliquots of their different concentrations were incubated with cells and cells only as controls for 48 hr. As seen in **Figure 7**, the viability of both cells was >80%, suggesting non-cytotoxicity up to 280 µg/mL.
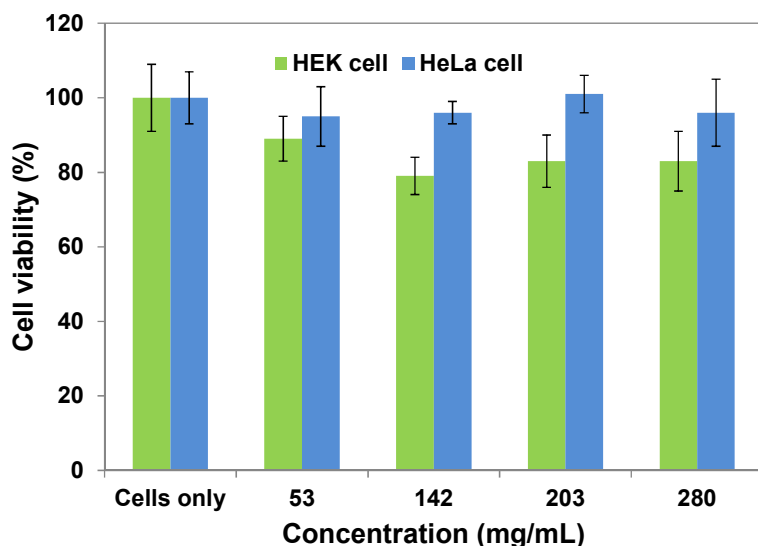
Figure 7. Viability of HEK 293T and HeLa cells cultured with various concentrations of aqueous SNP/BCP-HY micelles at 37 °C for 48 hrs, determined by MTT assay.

Colloidal stability of aqueous SNP/BCP-HY-45 micelles. For the analysis of surface properties, particularly surface charge of aqueous SNP/BCP-HY-45 micelles (containing acidic cores), zeta (ξ) potential was measured at various pH = 3-11 in 10 mM saline solution. As seen in **Figure 8a**, the ξ was close to zero at pH <4 (acidic pH) and gradually decreased to -15 mV as pH increased to pH = 11 (alkali pH). Particularly, it ranged at -10 mM at physiological pH range of 7-7.4, suggesting negative surface charge. This can be plausibly due to the presence of multiple pendant carboxylic acid groups in

their anionic forms (COO⁻) at the pH range. For comparison, the ξ of neutral SNP/BCP-HY-0 micelles was close to zero (<-3 mV).

A potential concern for the negatively-charged surface of SNP/BCP-HY-45 micelles is its interactions with proteins in serum, which is undesirable for prolonged blood circulation. Albumin is one of the most abundant protein available in the blood serum at the concentration ranging between 35-52 g/L.[49] Here, aliquots of SNP/BCP-HY-45 micelles were incubated with different amounts of BSA as the mass ratios of micelles/BSA = 1/40 and 1/1 in PBS at pH = 7.4, at 37 °C (to mimic physiological conditions). After 48 hrs of incubation, DLS diagrams show monomodal size distributions with no occurrence of significant aggregation (**Figure S7**). Further, to quantify the amount of BSA in supernatant, BCA assay was conducted. As seen in **Figure 8b,** SNP/BCP-HY-45 micelles exhibit great colloidal stability of SNP/BCP-HY-45 in the presence of proteins, suggesting no significant interactions with proteins.
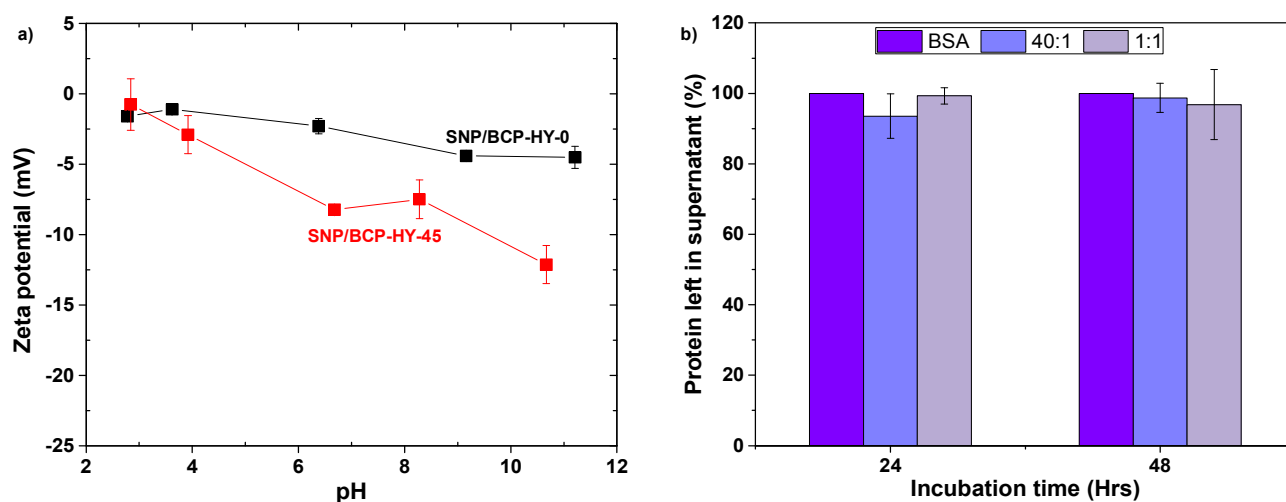
Figure 8. For SNP/BCP-HY-45 micelles, zeta potential over pH in10 mM saline solution to analyze surface properties (a) and percentage of free BSA in supernatants of mixtures at different mass ratios of micelle/BSA = 1/40 and 1/1after 24 and 48 hrs of incubation determined by BCA assay (b).

Next, shelf-stability of aqueous SNP/BCP-HY-45 micelles in various pH conditions was examined. Their equal volumes were mixed with KHP buffer (pH = 3 and pH = 5), PBS (pH = 7.4 and pH = 9), and then incubated at 37 °C for 18 hrs. DLS was used to follow any change in the size distribution of these mixtures. As seen in **Figure 9a**, DLS diagrams at pH = 7 and higher show no change in size with monomodal size distributions. Greater colloidal stability in biologically relevant conditions is highly essential to ensure not only prolonged circulation time, but also enhanced relaxometric properties for

MRI. Interestingly, at slightly acidic pH = 5, the size distribution become multimodal with the occurrence of significant aggregation. Further decrease of pH to 3 resulted in the precipitation of micelles (**Figure 9b** digital image). The plausible reason could be attributed to the presence of pendant acid groups in partially hydrolyzed P(tBMA-MAA) blocks. Since pKa of carboxylic acid = 4.8, most pendant acid groups in the cores could exist as their neutral forms (COOH); thus, their binding isotherms to metal surfaces can become weaker, causing the destabilization of SNP/BCP-HY-45 micelles based on PEO-b-P(tBMA-co-MAA) copolymers. Such acidic pH-responsive destabilization suggests the potential of SNP/BCP-HY-45 micelles exhibiting the enhanced release of encapsulated drugs.
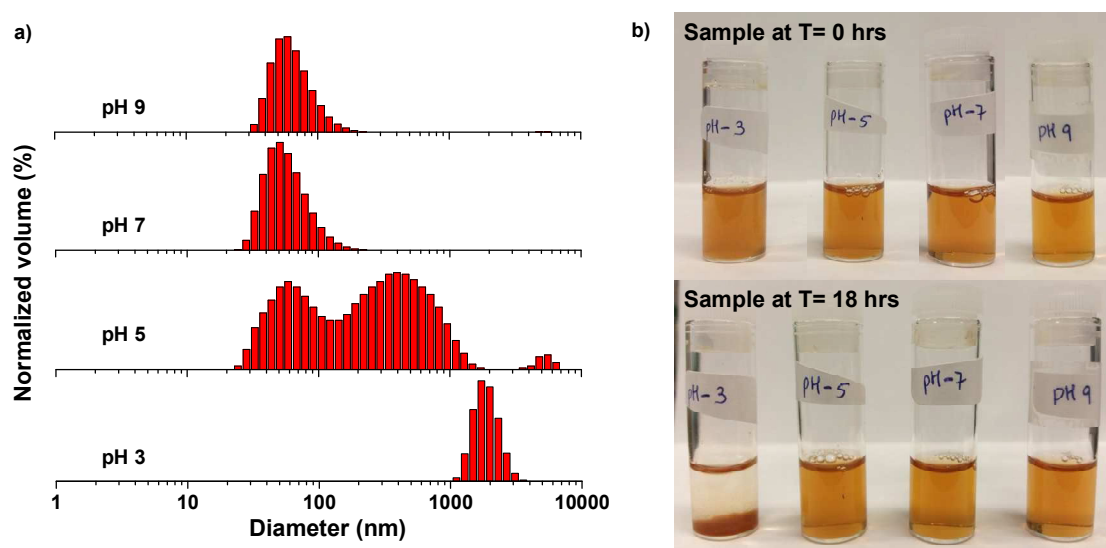
Figure 9. DLS histograms (a) and digital images (b) of aqueous SNP/BCP-HY-45 micelles incubated at pH = 3-9 over 18 hrs.

Loading and acidic pH-responsive release of anticancer drug. To preliminarily asses the BCP-HY-45 toward acidic pH-responsive drug delivery application, doxorubicin (Dox), a DNA-intercalating anti-cancer drug used in chemotherapy, was loaded in hydrophobic micellar cores. After intensive dialysis to remove free (not encapsulated) Dox, colloidally-stable Dox-loaded micelles in aqueous solution at 1.9 mg/mL were prepared. From the UV/vis spectrum of the Dox-loaded micelles (**Figure S8**) and the pre-determined extinction coefficient of Dox = 12,400 M^{-1} cm^{-1} at λ_{max} = 497 nm in a mixture of DMF/water = 5/1 (wt/wt),[50] the loading level of Dox was determined to be 2.6 %.

Next, the release of Dox from Dox-loaded micelles in response to acidic pH was examined. Aliquots of Dox-loaded micelles in dialysis tubing were placed in outer water at pH = 5 and 7 (control)

and the fluorescence spectra of the outer water were monitored over time (**Figure S9**). As summarized in **Figure 10**, fluorescence intensity at 597 nm increased over time at both pHs, suggesting the gradual release of encapsulated Dox from micelles over time. Importantly, Dox release was faster at pH = 5, compared to pH = 7. Such enhanced release at pH = 5 can be attributed to two reasons. One reason would be less interaction between Dox and acidic core-containing micelles as reported. [51, 52] At neutral pH = 7, amine groups of DOX molecules exist as protonated forms (NH_3^+ forms) because of pKa of Dox = 8.3, while carboxylic acid groups in micelles exist as anionic COO^- forms (note pKa of COOH = 4.3). Such relatively strong electrostatic interactions between Dox and micelles slow down Dox release. However, at pH = 5 (close to pKa of COOH), more carboxylic acid groups could exist as their neutral forms (COOHs). This could decrease the electrostatic interactions between Dox and micelles. Another would be instability of BCP-HY-45 micelles. At pH = 5, the micelles became destabilized with the occurrence of aggregation (**Figure S10**).
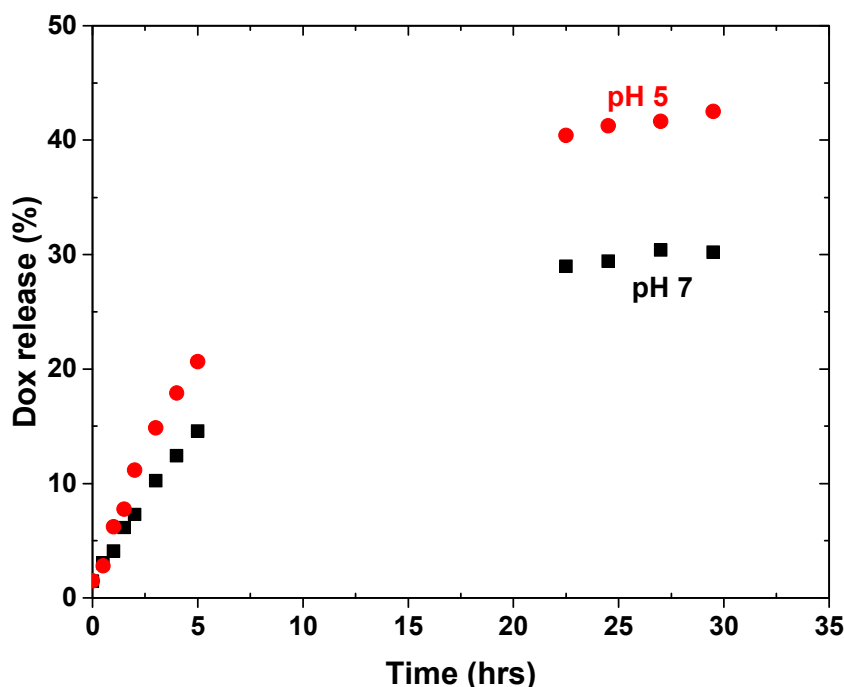
Figure 10. Acidic pH-responsive release of Dox from Dox-loaded BCP-HY-45 micelles in aqueous solution at pH = 5, compared with pH = 7.4.

CONCLUSIONS

Well-controlled BCP-HY [PEG-b-P(tBMA-co-MAA)] amphiphilic block copolymer with pendant COOH groups were synthesized by ATRP to neutral PEG-b-PtBMA precursor, followed by partial

hydrolysis of pendant t-butoxy groups in the presence of an acid. At concentrations above CMC = 6 - 20 µg/mL, they self-assembled in aqueous solution to form micellar aggregates having acidic cores composed of COOH groups. The introduction of COOH groups to hydrophobic cores enhanced the loading level of SNPs by 20%, compared with the neutral counterpart (PEG-b-PtBMA based micelles). Such higher loading is attributed to their ability to anchor to SNP surfaces. As a consequence, the resultant SNP/HCP-HY acidic micelles exhibit T_2-wighted MRI contrast enhancement; however, the r_2 relaxivity constant increased with the micelle size. They were colloidally stable in the presence of BSA (a model protein found in serum) even though they had negative zeta potential ranging at -10 and -15 mV at physiological pH range of 7-7.4. They also show good shelf-stability at pH >7, but were destabilized at acidic pH. Promisingly, they exhibit the enhanced release of encapsulated anticancer drug upon acidic pH-response. These results suggest that SNP/BCP-HY micelles loaded with anticancer drugs could have potential as multifunctional theranostic platform for simultaneous drug delivery and molecular imaging application.

ACKNOWLEDGMENT

REFERENCE

1. Y. Gossuin, P. Gillis, A. Hocq, Q. L. Vuong and A. Roch, *Wiley Interdiscip. Rev. Nanomed. Nanobiotechnol.* 2009, **1**, 299.
2. E. Amstad, M. Textor and E. Reimhult, *Nanoscale* 2011, **3**, 2819.
3. J. Huang, X. Zhong, L. Wang, L. Yang and H. Mao, *Theranostics* 2012, **2**, 86.
4. N. Lee and T. Hyeon, *Chem. Soc. Rev.* 2012, **41**, 2575.
5. C. Sun, J. S. H. Lee and M. Zhang, *Adv. Drug Delivery Rev.* 2008, **60**, 1252.
6. W. Chen, D. P. Cormode, Z. A. Fayad and W. J. M. Mulder, *Wiley Interdiscip. Rev. Nanomed. Nanobiotechnol.* 2011, **3**, 146.
7. M. E. Lobatto, V. Fuster, Z. A. Fayad and M. J. M. Mulder, *Nat. Rev. Drug Discovery* 2011, **10**, 835.
8. J. K. Oh and J. M. Park, *Prog. Polym. Sci.* 2011, **36**, 168.
9. F. Hu, Q. Jia, Y. Li and M. Gao, *Nanotechnology* 2011, **22**, 245604/1.
10. B. H. Kim, N. Lee, H. Kim, K. An, Y. I. Park, Y. Choi, K. Shin, Y. Lee, S. G. Kwon, H. B. Na, J.-G. Park, T.-Y. Ahn, Y.-W. Kim, W. K. Moon, S. H. Choi and T. Hyeon, *J. Am. Chem. Soc.* 2011, **133**, 12624.

11.   L. Sandiford, A. Phinikaridou, A. Protti, L. K. Meszaros, X. Cui, Y. Yan, G. Frodsham, P. A. Williamson, N. Gaddum, R. M. Botnar, P. J. Blower, M. A. Green and R. T. M. de Rosales, *ACS Nano* 2013, **7**, 500.

12.   U. I. Tromsdorf, O. T. Bruns, S. C. Salmen, U. Beisiegel and H. Weller, *Nano Lett.* 2009, **9**, 4434.

13.   J. Y. Park, P. Daksha, G. H. Lee, S. Woo and Y. Chang, *Nanotechnology* 2008, **19**, 365603/1.

14.   F. Hu and Y. S. Zhao, *Nanoscale* 2012, **4**, 6235.

15.   H. B. Na, I. C. Song and T. Hyeon, *Adv. Mater.* 2009, **21**, 2133.

16.   H. Duan, M. Kuang, X. Wang, Y. A. Wang, H. Mao and S. Nie, *J. Phys. Chem. C* 2008, **112**, 8127.

17.   J. Qin, S. Laurent, Y. S. Jo, A. Roch, M. Mikhaylova, Z. M. Bhujwalla, R. N. Muller and M. Mohammed, *Adv. Mater.* 2007, **19**, 1874.

18.   H. B. Na, G. Palui, J. T. Rosenberg, X. Ji, S. C. Grant and H. Mattoussi, *ACS Nano* 2012, **6**, 389.

19.   Y. Zhong, F. Dai, H. Deng, M. Du, X. Zhang, Q. Liu and X. Zhang, *J. Mater. Chem. B* 2014, **2**, 2938.

20.   J. S. Basuki, A. Jacquemin, L. Esser, Y. Li, C. Boyer and T. P. Davis, *Polym. Chem.* 2014, **5**, 2611.

21.   M. Boularas, E. Gombart, J. F. Tranchant, L. Billon and M. Save, *Macromol. Rapid Commun.* 2015, **36**, 79.

22.   B.-S. Kim, J.-M. Qiu, J.-P. Wang and T. A. Taton, *Nano Lett.* 2005, **5**, 1987.

23.   X. Pan, J. Guan, J. W. Yoo, A. J. Epstein, L. J. Lee and R. J. Lee, *Int J Pharm* 2008, **358**, 263.

24.   J. Park, S. Park, S. Kim, I.-H. Lee, P. E. Saw, K. Lee, Y.-C. Kim, Y.-J. Kim, O. C. Farokhzad, Y. Y. Jeong and S. Jon, *J. Mater. Chem. B* 2013, **1**, 4576.

25.   M. Fan, J. Yan, H. Tan, Y. Miao and X. Hu, *J. Mater. Chem. B* 2014, **2**, 8399.

26.   G. Wang, X. Zhang, Y. Liu, Z. Hu, X. Mei and K. Uvdal, *J. Mater. Chem. B* 2015, **3**, 3072.

27.   C. Wang, H. Xu, C. Liang, Y. Liu, Z. Li, G. Yang, L. Cheng, Y. Li and Z. Liu, *ACS Nano* 2013, **7**, 6782.

28.   M. B. Bannwarth, A. Camerlo, S. Ulrich, G. Jakob, G. Fortunato, R. M. Rossi and L. F. Boesel, *Chem. Commun.* 2015, **51**, 3758.

29.   S. S. Kelkar and T. M. Reineke, *Bioconjugate Chem.* 2011, **22**, 1879.

30.   S. Mura and P. Couvreur, *Adv. Drug Deliv. Rev.* 2012, **64**, 1394.

31.   H. Ai, C. Flask, B. Weinberg, X. Shuai, M. D. Pagel, D. Farrell, J. Duerk and J. Gao, *Adv. Mater.* 2005, **17**, 1949.

32.   P. Arosio, J. Thévenot, T. Orlando, F. Orsini, M. Corti, M. Mariani, L. Bordonali, C. Innocenti, C. Sangregorio, H. Oliveira, S. Lecommandoux, A. Lascialfari and O. Sandre, *J. Mater. Chem. B* 2013, **1**, 5317.

33.   J. Lu, S. Ma, J. Sun, C. Xia, C. Liu, Z. Wang, X. Zhao, F. Gao, Q. Gong, B. Song, X. Shuai, H. Ai and Z. Gu, *Biomaterials* 2009, **30**, 2919.

34.   S.-M. Lai, J.-K. Hsiao, H.-P. Yu, C.-W. Lu, C.-C. Huang, M.-J. Shieh and P.-S. Lai, *J. Mater. Chem. B* 2012, **22**, 15160.

35.   C. Gonçalves, Y. Lalatonne, L. Melro, G. Badino, M. F. M. Ferreira, L. David, C. F. G. C. Geraldes, L. Motte, J. A. Martins and F. M. Gama, *J. Mater. Chem. B* 2013, **1**, 5853.

36.   Y. Lin, S. Wang, Y. Zhang, J. Gao, L. Hong, X. Wang, W. Wu and X. Jiang, *J. Mater. Chem. B* 2015, **3**, 5702.

37.   D. Smejkalova, K. Nesporova, G. Huerta-Angeles, J. Syrovatka, D. Jirak, A. Galisova and V. Velebny, *Biomacromolecules* 2014, **15**, 4012.

38.   G. L. Davies, I. Kramberger and J. J. Davis, *Chem. Commun.* 2013, **49**, 9704.

39.   M. Ding, X. Zeng, X. He, J. Li, H. Tan and Q. Fu, *Biomacromolecules* 2014, **15**, 2896.

40. X. Zhu, S. Chen, Q. Luo, C. Ye, M. Liu and X. Zhou, *Chem. Commun.* 2015, **51**, 9085.
41. S. Aleksanian, Y. Wen, N. Chan and J. K. Oh, *RSC Adv.* 2014, **4**, 3713.
42. G. J. P. Britovsek, J. England and A. J. P. White, *Inorg. Chem.* 2005, **44**, 8125.
43. N. Chan, M. Laprise-Pelletier, P. Chevallier, A. Bianchi, M.-A. Fortin and J. K. Oh, *Biomacromolecules* 2014, **15**, 2146.
44. Q. Ma and K. L. Wooley, *J. Polym. Sci., Part A Polym. Chem.* 2000, **38**, 4805.
45. A. Cunningham and J. K. Oh, *Macromol. Rapid Commun.* 2013, **34**, 163.
46. N. Chan, N. Yee, S. Y. An and J. K. Oh, *J. Polym. Sci., Part A Polym. Chem.* 2014, **52**, 2057.
47. H. B. Na, I. C. Song and T. Hyeon, *Advanced Materials* 2009, **21**, 2133.
48. R. Barbieri, M. Quaglia, M. Delfini and E. Brosio, *Polymer* 1998, **39**, 1059.
49. Y. Wen and J. K. Oh, *Colloids Surf B Biointerfaces* 2015, **133**, 246.
50. N. Chan, S. Y. An and J. K. Oh, *Polym. Chem.* 2014, **5**, 1637.
51. Y. Wen and J. K. Oh, *Colloids Surf. B* 2015, **133**, 246.
52. Y. Wen and J. K. Oh, *RSC Adv.* 2014, **4**, 229.

457x141mm (72 x 72 DPI)